Aβ1-42 peptide toxicity on neuronal cells: A lipidomic study

Aß$_{1-42}$ peptide toxicity on neuronal cells: a lipidomic study

Lara Davani,[1] Xiaoqing Fu,[2] Angela De Simone,[3] Peng Li,[2] Serena Montanari,[1] Michael Lämmerhofer,[2] and Vincenza Andrisano[1] *

[1] Department for Life Quality Studies, University of Bologna, Corso D' Augusto 237, 47921 Rimini, Italy;

[2] Institute of Pharmaceutical Sciences, University of Tuebingen, Auf der Morgenstelle 8, 72076 Tuebingen, Germany;

[3] Department of Drug Science and Technology University of Torino, via P.Giuria 9, 10125 Torino, Italy.

***Author for correspondence:**
Prof. Vincenza Andrisano
Department for Life Quality Studies
University of Bologna
Corso D' Augusto 237
47921 Rimini, Italy
e-mail: vincenza.andrisano@unibo.it

Abstract

Currently Alzheimer's Disease (AD) pathological pathways, which lead to cell death and dementia, are not completely well-defined; in particular, the lipid changes in brain tissues that begin years before AD symptoms. Due to the central role of the amyloid aggregation process in the early phase of AD pathogenesis, we aimed at developing a lipidomic approach to evaluate the amyloid toxic effects on differentiated human neuroblastoma derived SH-SY5Y cells. First of all, this work was performed to highlight qualitative and relative quantitative lipid variations in connection with amyloid toxicity. Then, with an open outcome, the study was focused to find out some new lipid-based biomarkers that could result from the interaction of amyloid peptide with cell membrane and could justify neuroblastoma cells neurotoxicity.

Hence, cells were treated with increasing concentration of $Aß_{1-42}$ at different times, then the lipid extraction was carried out by protein precipitation protocol with 2-propanol-water (90:10 v/v). The LC-MS analysis of samples was performed by a RP-UHPLC system coupled with a quadrupole-time-of-flight mass spectrometer in comprehensive data - independent SWATH acquisition mode. Data processing was achieved by MS-DIAL. Each lipid class profile in SH-SY5Y cells treated with $Aß_{1-42}$ was compared to the one obtained for the untreated cells to identify (and relatively quantify) some altered species in various lipid classes. This approach was found suitable to underline some peculiar lipid alterations that might be correlated to different $Aß_{1-42}$ aggregation species and to explore the cellular response mechanisms to the toxic stimuli. The *in vitro* model presented has provided results that coincide with the ones in literature obtained by lipidomic analysis on cerebrospinal fluid and plasma of AD patients. Therefore, after being validated, this method could represent a way for the preliminary identification of potential biomarkers that could be researched in biological samples of AD patients.

Keywords: Alzheimer's Disease, Amyloid Toxicity, Lipids, Mass Spectrometry, Biomarkers

1. Introduction

Alzheimer's disease (AD) is the most common type of dementia and is a growing global health concern with huge implications for individuals and society. In 2019 the Alzheimer's Disease International Association (ADI) estimated over 50 million people living with dementia worldwide, and due to the gradual ageing of the population its incidence is expected to increase up to 152 million in 2050 [1]. AD is a neurodegenerative disease clinically characterized by a progressive memory loss, cognitive dysfunction and behavioural change. The major neuropathological hallmarks of AD are amyloid plaques, consisting of β-amyloid peptide (Aβ), and neurofibrillary tangles (NFTs) primarily composed of paired helical filaments of hyperphosphorylated tau. In addition, dystrophic neurites, associated astrogliosis, and microglial activation are detected in AD patients. Furthermore, cerebral amyloid angiopathy frequently coexists.

The amyloid hypothesis, firstly formulated in the early 1990s, proposed that an abnormal extracellular increase of Aß peptide levels in the brain could lead to Aß aggregation into ß-sheet rich structures. Amyloid monomers are derived from the amyloid precursor protein (APP) found on the surfaces of many cells, including neurons. In the pathway to Aß formation, APP undergoes proteolysis by ß-secretase, the ß-site APP cleaving enzyme 1 (BACE1), and γ-secretase to form Aß fragments. There are two major species of Aß in the brain: $Aß_{1-42}$ and $Aß_{1-40}$. Although $Aß_{1-40}$ is several times more abundant than $Aß_{1-42}$ in soluble form, $Aß_{1-42}$ is the major constituent of amyloid plaques [2]. Aggregation starts precisely with the formation of oligomers species that are reorganized into protofibrils and fibrils, the latter found in amyloid plaques.

Currently, a leading strategy appears to be diagnosing and treating Alzheimer's disease in the early stages. This could stop the gradual worsening of the symptoms; thus it is crucial to research biomarkers involved at the onset of AD neurodegeneration. Among the biomarkers identified in cerebrospinal fluid and used for the diagnosis of Alzheimer's disease, $Aß_{1-42}$ peptide seems the most sensitive one. Specifically, $Aß_{1-42}$ oligomers accumulated in the brain of AD patients are suggested to be the most toxic species for neurons. $Aß_{1-42}$ is a relatively hydrophobic peptide as figured out from its amino acid sequence, and the $Aß_{1-42}$ oligomers solubilize into the hydrophobic environment of the lipid bilayer of the neuronal membrane [3]. Then, they adopt an α-helical secondary structure into the membrane-spanning region of the peptide, as almost all proteins that solubilize in a lipid bilayer do. Cell membranes are constituted by phospholipids (glycerophospholipids and sphingolipids) which influence the behaviour of membrane proteins, receptors, enzymes and ion

channels both at the intracellular level or on the cell surface. Therefore, it is assumed that any changes in the brain phospholipids trigger pathogenic mechanisms. The exact mechanism by which amyloid peptide determines brain dysfunction in AD patients is not yet clarified. However, one hypothesis exists, and it is based on the interaction with neuronal plasma membranes, whose mechanism has already been described by model lipid systems, at least partially [4]. Although several processes have been proposed, what is sure is the subsequent Aβ peptide aggregation and the Ca^{2+} permeability perturbation after the interaction. The latter results either from a channel-independent mechanism (formation of Ca^{2+} pores) or from a channel-dependent one (through NMDA-R and AMPA-R) [5]. Therefore, developing a lipidomic method for monitoring cell lipid profile changes in response to Aβ oligomers stimulus could discover new potential AD biomarkers.

Indeed, due to the role of lipid dyshomeostasis in AD pathogenesis, now lipidomics is an emerging research field [6–8]. Moreover, brain lipidomics was useful to unravel the altered lipid profile in neurons and glial cells as well as biofluids such as cerebrospinal fluid (CSF) and plasma [9–13]. Concerning biofluids, the main limitation of researching CSF biomarkers is that CSF sampling requires a lumbar puncture that is invasive and dependent on considerable medical skill and so it cannot be applied to general screening or for repeat measures. Investigating lipidic peripheral changes, they result much more convenient: blood is easier to extract, relatively risk free, unexpensive, and suitable for repeated sampling. Although blood is a secondary compartment for brain related molecules, through the blood–brain barrier (BBB) partition, CSF exchanges metabolites with blood during the reabsorption into the vascular system, moreover BBB permeability may increase in some conditions. A substantial overlap in metabolic changes identified in CSF and plasma has been demonstrated, therefore it may be possible to detect brain-related alterations to lipid profiles by examining blood-based biomarkers. [14]

Lipidomic studies can now take advantage of sensitive and robust analytical approaches based on the use of liquid chromatography-electrospray ionisation-mass spectrometry (LC-ESI-MS) systems. These methods made possible to analyse most of the lipids in the same assay, in a rapid and sensitive way. Indeed, NMR spectroscopy has demonstrated to be a powerful technology in metabolite analysis of body fluids, cells and intact tissues. It has strong quantitative capabilities, but the sensitivity of NMR is limited compared to MS-based approaches in complex mixtures: MS is able to determine different phospholipid classes simultaneously using a small amount of sample. Therefore, recent publications have focused more on MS-based technologies rather than NMR, especially when

dealing with very low abundant samples. Moreover, a turning point in lipidomics has been the introduction of soft ionization technologies, such as: matrix assisted laser desorption / ionization (MALDI), ESI and atmospheric pressure chemical ionization (APCI) for MS, possibly coupled to liquid chromatography (LC). In fact, gas chromatography (GC) has been, and still is, often used for lipid analysis, but time-consuming procedures (i.e. hydrolysis and derivatization) are usually required since most lipids are otherwise not susceptible to GC. Nowadays, GC coupled with mass spectrometry is mainly used for full comprehensive fatty acid profiling as fatty acid methyl esters (FAMEs).

Specifically, as for the brain lipid alterations known in AD patients, it seems that phospholipids, which are the main components of cell membrane, are involved in the pathogenesis

Therefore, further studies might clarify the connections existing between Aβ aggregation species and the alterations in brain lipid metabolism. In this context, the most crucial steps of the proposed project, that is based on previous studies on amyloid aggregation [15,16], concern differentiated SH-SY5Y cells treatment with $A\beta_{1-42,}$ and the development of a LC-MS method to analyse the cell lipids. Combining the lipid profile analysis with with univariate and multivariate statistics in a lipidomic approach can help monitor some lipid changes connected to Aβ peptide toxicity in order to uncover potential biomarkers that might be correlated to specific type of $Aß_{1-42}$ aggregation species. In the meantime, the developed method can support the investigation of cellular response mechanisms to the amyloid toxic stimuli and finally it could contribute to new hypotheses about the mechanisms of in-depth lipid-mediated disease. The perspective is using this *in vitro* model to identify new tentative biomarkers which after their clinical validation, could be useful or supportive for AD diagnosis, prognosis prediction, or monitoring of therapeutical effects in biological samples.

2. Material and methods

2.1 Material

Mobile phases were prepared with solvents of Ultra LC-MS grade. Acetonitrile (ACN) and isopropanol (IPA) were supplied by Carl Roth (Karlsruhe, Germany). Ammonium formate, formic acid, and IPA of HPLC grade, were purchased from Merck (Darmstadt, Germany). Ultrapure water was obtained by purification with a water filtration system from Elga Purelab (Celle, Germany).

EquiSPLASH™ LIPIDOMIX® containing the following isotopically labeled internal standards (ILIS): 15:0e-18:1(d7)-PC, 15:0-e18:1(d7)-PE, 15:0e-18:1(d7)-PS, 15:0e-18:1(d7)-PG, 15:0e-18:1(d7)-PI, 15:0e-18:1(d7)-PA, 18:1(d7)-LPC, 18:1(d7)-LPE, 18:1(d7)-Chol Ester, 18:1(d7)-MG, 15:0e-18:1(d7)-

DG, 15:0e-18:1(d7)-15:0-TG, 18:1(d9)-SM, Cholesterol(d7) was purchased from Avanti Polar Lipids (Alabaster, AL, USA). Arachidonic acid-d11 (AA-d11), C18-Ceramide-d7 (d18:1-d7/18:0), and Palmitoyl-L-Carnitine (d3) were obtained from Cayman Chemicals (Ann Arbor, MI, USA). The final concentrations used are specified in Supplementary Table S1. Light Splash containing the following standards: 15:0-18:1 PC, 18:1 Lyso PC , 15:0-18:1 PE, 18:1 Lyso PE, 15:0-18:1 PG, 15:0-18:1 PI , 15:0-18:1 PS, 15:0-18:1-15:0 TG, 15:0-18:1 DG, 18:1 MG, 18:1 Chol Ester, d18:1-18:1 SM and C15 Ceramide (d18:1/15:0) was acquired from Avanti Polar Lipids; FA 20:4 (AA), Palmitoyl-L-Carnitine, FA 15:0-18:1 (PA), Cholesterol, Chol Ester 18:1, d18:1 Lyso SM and Sphingosine-1-phosphate d18:1 were obtained from Cayman Chemicals. The concentrations of unlabeled standards used as calibrants in QC samples for the method validation are listed in Supplementary Table S3.

2.2 Aβ$_{1-42}$ peptide preparation

One mg of Aβ$_{1–42}$ lyophilized (Bachem, Bubendorf, Switzerland) powder was pretreated overnight with 1400 µL of hexafluoroisopropanol (HFIP) (Merck Life Science S.r.l; Milan, Italy), aliquoted, and the resulting unaggregated Aβ$_{1–42}$ peptide film was stored at −20 °C after solvent evaporation.
Before cell treatment, Aβ$_{1-42}$ film was dissolved in 40 µL of DMSO (Merck Life Science S.r.land left at room temperature for 1 h, then diluted in Dulbecco's Phosphate Buffered Saline (PBS) (Euroclone; Milan, Italy) to reach the final concentration of 500 µM.

2.3 Cell culture and cell treatment

The cells used throughout these experiments were human neuronal cells, SH-SY5Y (Merck Life Science S.r.l). Cells were grown in Dulbecco's modified Eagle's Medium (DMEM) supplemented with 10% heat-inactivated fetal bovine serum (FBS), 1% 2 mM L-glutamine solution and 1% penicillin/streptomycin solution (Euroclone). Cells were incubated at 37° C in a humidified incubator with 5% CO_2. To maintain exponential growth, the medium was changed every 2 – 3 days and cells were split using 0.025 % Trypsin-EDTA solution (Euroclone). Cells were then seeded in 24 well culture plate at a concentration of 2.5 – 5 – 10 - 15 x 10^4 cells/well. Cells were used for experiments after inducing their differentiation with RA. After 4 h from seeding, Retinoic Acid (AR) (Euroclone) at final concentration of 10 µM in DMEM was added. Cells were incubated for a total of four days with RA, changed every 48h. Human brain derived neurotrophic-factor (BDNF) (Euroclone) at the final concentration of 50 ng/mL was added in fresh DMEM without FBS for at least two days. The

cells differentiated were then used for the treatment with $A\beta_{1-42}$ at different concentrations (2-5-10-25-40-50 µM).

After 24h or 48h incubation (different treatment time), the cell viability was evaluated and then the cells were washed with 500 µL of PBS. Afterwards, the cells were incubated with 100 µL of Trypsin solution (0.025%) at 37°C. After 3 min, cells were washed by adding 300 µL of DMEM supplemented with 10% fetal bovine serum.

The suspension was transferred into 1.5 mL reaction tubes and centrifuged at 1200 rpm for 5 min at 25 °C; the supernatant was withdrawn. The remaining cell pellets were frozen at –20 °C until extraction.

2.4 Cell Viability Measurement

Cell viability was evaluated using the PrestoBlue™ HS Cell Viability Reagent. It is a ready-to-use resazurin-based solution that works as a cell health indicator by using the reducing power of living cells to quantitatively measure viability. This reagent has been optimized for the fast and reliable detection of mammalian cell viability. Resazurin-based reagent enters the living cells that continuously converts resazurin to resorufin, resulting in a pronounced color change. Thus, the cell viability can be detected using absorbance-based plate readers. Since no lysis is required, the diluted PrestoBlue HS solution can be removed and replaced with complete growth medium, for further culturing of the cells. So, briefly, at the end of each experiment, the cell medium was removed, and replaced by a mix of 450 µL of complete growth media and 50 µL of PrestoBlue™ HS Cell Viability Reagent in each well of the 24-well plate. After 3h of incubation at 37 °C and 5% CO_2, the absorbance at 570 nm was detected through microplate spectrophotometer (VICTOR3 V Multilabel Counter; PerkinElmer, Wellesley, MA, USA) using 600 nm as reference wavelength. Data are reported as percentage with respect to controls. Control cells are considered as 100 % cell viability (Fig. 1).

2.5 Lipid Extraction of samples

Before starting the extraction, the internal standard (IS) mix and cell pellet samples were stored on ice. Prior pipetting, the IS solution was completely dissolved, vortexing (10 s), ultrasonicating 2 min and vortexing again (10 s), ice was added to the ultrasonic bath for cooling. Then, cell pellets were spiked with 100 µL of internal standard (IS) mix and they were vortexed (30 s). Finally, 1 mL of IPA:H_2O (90:10 v/v) extractive solution, was added and samples were vortexed (30 s) again. During the entire process the samples and the extraction solvent were stored on ice.

Afterwards, five (5) cycles (6500 rpm x 10 s and 30 s of pause between each other, 4°C) in Precellys® evolution homogenizer (Bertin GMBH, Frankfurt am Main, Germany) were applied for the cell cryo-lysis. Then samples were incubated on ice on an orbital shaker (500 rpm, 60 min) to have a complete protein precipitation and lipid extraction. After the lipid extraction, centrifugation at 12,200 rpm for 10 min was applied and the supernatant was transferred to a 1.5 mL reaction tube. Samples were dried overnight by a high-performance evaporator (GeneVac EZ2 evaporator, Ipswich, United Kingdom) with nitrogen protection. The lipid extract was reconstituted in 100 µL of methanol followed by vortexing (30 sec) and sonication (2 min). Centrifugation at 3500 rcf for 3 min at 4°C was performed and the supernatants were transferred into vials for MS-measurements. During the last step, 10 uL aliquot from each sample was removed and transferred into another vial to prepare the pooled QC sample.

2.6 LC-MS/MS Untargeted Analysis

Analyses were performed by Agilent 1290 Series UHPLC instrument (Agilent, Waldbronn, Germany) coupled to Sciex Triple-TOF 5600+ MS (Sciex, Vaughan, Canada) with duo-spray source and Pal HTC-xt autosampler from CTC (Zwingen, Switzerland). All samples were analyzed in both positive and negative ion mode with electrospray ionization with the same chromatographic separation conditions.

Acquity UPLC CSH C18 (130 Å, 1.7 µm, 2.1 mm × 100 mm) column was used with Acquity UPLC CSH C18 VanGuard pre-column (130 Å, 1.7 µm, 2.1 mm × 5 mm) (Waters, Eschborn, Germany) for chromatographic separation [17].

About the mobile phase, eluent A was composed of 60:40 ACN:H2O (v/v) containing 10 mM ammonium formate and 0.1% formic acid (v/v) and eluent B of 90:9:1 IPA/ACN/H2O (v/v/v) containing 10 mM ammonium formate and 0.1% formic acid (v/v). The gradient elution started with 15% B; then it was increased to 30% B in 2 min followed by further increase to 48% B within the next 0.5 min. In the following 11.00 min the gradient was elevated to 82% B and then quickly reached 99% B in the next 0.5 min, and stayed at this percentage for 0.5 min; afterwards, the percentage of B was set to starting conditions (15% B) in 0.1 min to re-equilibrate the column for the next injection (2.9 min). The flow rate was 0.6 mL/min and column temperature was 65 °C. The injection volumes were 3 µL and 5 µL for positive and negative ion mode, respectively.

LC-ESI-MS/MS experiments were measured firstly in positive polarity mode and then in negative polarity mode. The mass spectrometry parameters were set as follows: curtain gas (CUR) 35 psi, nebulizer gas (GS1) 60 psi, drying gas (GS2) 60 psi, ion-spray voltage floating (ISVF) + 5500 V in positive and - 4500 V in negative mode, source temperature (T) 350 ° C, collision energy 45 V, collision energy spread 15 V, declustering potential (DP) 80 V, mass range m/z 50-1250 in ESI (+) and m/z 50-1050 in ESI (-), and RF Transmission (RF) m/z 40: 50% and m/z 120: 50%.

MS/MS experiments were acquired by using sequential window acquisition of all theoretical fragment ion mass spectra (SWATH). The MS cycle time was always 720 ms. More details on MS and MS/MS experiments are reported in S.I. (Table S6).

The sample order was randomized. The sequence started with three injections of IS mixture as system suitability test and was controlled by regular injection of the QC sample after every 5 samples to control the performance of the instrument throughout the sequence. The carry-over effect was checked during method validation by injecting blank solution after QC sample (data related to method validation are available in the S.I.). The response in blank sample meets the requirement of FDA guideline (not exceed 20% of LLOQ) Finally, a dilution series of calibrant solution has been injected at the beginning and in the end of the sequence.

2.7 Lipidomic Data Processing

2.7.1 Preprocessing and structural annotation based on MS data and MS/MS spectral match

MultiQuant 3.0 software was used to calculate the peak height of the IS while data pre-processing, identification and relative quantification of the unknown lipids were performed using MS-Dial software (RIKEN, version 4.24) [18]. Data raw files (.wiff format) were converted into Analysis Base Files (.abf format) via the ABF converter (Reifycs, Tokyo, Japan) in order to perform peak detection, deisotoping, adduct assignment, feature alignment, MS2 data deconvolution, and compound identification through all the samples. After conversion, the MS-DIAL projects were created separately for each ionization mode (Fig.2).

The identification was achieved by comparison of experimental spectra with those in the LipidBlast library (t_R tolerance for Lipid-Blast based identification: 0.5 min) using both accurate mass and MS/MS fragmentation data (identification score cut-off: 85%)

Processing parameters were adjusted to the following settings: peak finding between 0 and 15 min; precursor m/z range from 50 to 1250; TOF-MS and SWATH-MS/MS tolerance for peak profile were

set to 0.01 and 0.025 Da, respectively; Smoothing level: 1; minimum number of points per peak: 5; minimum peak height: 1000 cps.

Blank subtraction was exerted for signals that had a fold change <5 in the average samples compared to the average blank signals.

A pooled quality control sample (QC, a mix of all samples in the batch) was prepared and injected several times (every five samples) during the batch analysis to test the instrumental variability. Peak alignment was based on the 5th QC sample with a t_R tolerance of 0.2 min. TOF-MS tolerance of m/z 0.05.

2.7.2 Controlling for misannotations by retention time model

In reversed phase chromatography the different lipid species of the same class elute with a regular characteristic order. For this reason, retention time prediction models can be utilized to confirm lipid identification and check for mis-annotations, respectively. The retention time prediction model used here was based on two main observations. First, lipids of the same class with the same number of double bonds in the FAs elute in order of increasing carbon number (as sum of carbon atoms in FA chains). Secondly, lipids of the same class and the same number of carbons in FA chains elute in order of decreasing double bond number. All lipid classes were analyzed separately. In each class, lipids were divided into groups with the same number of double bonds. For each class, a spotting map, a plot of m/z of precursor ions versus retention times was prepared. Then, the empirical correlation of the given m/z and RT was calculated for each group. A correlation coefficient > 0.95 was required to consider that all the found lipids were correctly identified. However, if the correlation coefficient was lower or elution order was not correct, outliers were removed.

2.7.3 Relative quantification

Data of the lipids were normalized to the lipid class-specific IS. The relative abundance of every lipid species has been calculated as percentage distribution in its lipid class (sum of the total lipid signals identified in the same class).

Non-parametric Mann-Whitney U Test (U-test) was performed at significance level P=0.05. Fold changes were also calculated in the paired manner to find significantly regulated lipids between the two groups of treated cells and untreated control samples

3. Results and Discussion

3.1 Background and study design

In the present work differentiated neuroblastoma cells were treated with $A\beta_{1\text{-}42}$ peptide at increasing concentrations (2-50 μM) for 24 h and at 50 μM for 48 h, respectively, in the first and in the second case studies. The $A\beta_{1–42}$ peptide concentration and time of incubation were fixed in agreement with other previous studies [19,20].

The human SH-SY5Y cell line is widely used as a model for different neurodegenerative diseases. Due to their dopaminergic character, SH-SY5Y cells are generally considered as a model for Parkinson's disease [21]. However, their phenotype can be changed by different protocols of neural differentiation and to obtain dominantly cholinergic phenotype suitable for AD studies [22]. So far, the *in vitro* toxic effects of amyloid peptides are commonly examined using the human neuroblastoma derived SH-SY5Y cell line. However, in most of the publications non-differentiated cells are used. According to a recent study differentiation is a crucial step to achieve most accurate results for translation and comparison to *in vivo* models [23]. For this reason, in the present experiments, SH-SY5Y cells were treated with retinoic acid (RA) and brain-derived neurotrophic factor (BDNF), following the same protocol as described by Krishtal et al. [23]. In fact, differentiated neuron-like SH-SY5Y cells are more sensitive to amyloid peptides than non-differentiated cells, because the latter lack long neurites. It is known that the toxic effect of exogenous soluble $A\beta_{1–42}$ is related to its tendency to cover cell bodies and whole neurites in differentiated cells with dense fibrils, causing neurite beading and fragmentation. When SH-SY5Y cells are undifferentiated, they rapidly proliferate and appear to be non-polarized, with very few, short processes. They often grow in clumps and express markers indicative of immature neurons. Nevertheless, currently there are only a few studies examining Aβ-induced toxicity in differentiated SH-SY5Y cells. Moreover, only in a recent study Aβ-induced toxicity has been investigated in RA/BDNF differentiated SH-SY5Y cells [23].

Another important investigated issue concerns the exact nature and secondary structure of the toxic forms of Aβ. In 1994 Lambert and colleagues proved that the toxic effect of $A\beta_{1–42}$ on RA pre-treated SH-SY5Y cells could be attributed to the peptide oligomers (DMSO-induced) [24]. In agreement, in the study of Krishtal et al the preformed $A\beta_{1–42}$ fibrils had no toxic effects. The Andrisano research

group investigated through circular dichroism spectroscopy the influence of experimental conditions in determining the conformation and the solubility of Aβ *in vitro*, which in turn affects the rate of amyloid aggregation [25]. They also showed that the change of secondary structure towards β-sheets can be reverted by inhibitors [25]. They proved that the kinetic of the amyloid aggregation process is strongly related to the peptide and salt concentration in solution, the temperature, the pH value and solvent properties and concentration of active inhibitors. The storing conditions of the solid-state peptide were found to significantly affect its conformation too. For all these reasons, we used the validated method by Bartolini et al. to prepare $A\beta_{1–42}$ peptide with a high non-amyloidogenic conformation content. This is a crucial point to ensure that aggregation starts from the same Aβ conformation conditions. For this purpose, the Aβ peptide was solubilized in HFIP which represents an ideal solvent to stabilize the Aβ peptide in its α-helix secondary structure conformation even after 24 h. Then the resulting $A\beta_{1-42}$ film obtained by solvent evaporation was stable when kept at -20 °C and could be stored and used for further studies. Before the incubation with SH-SY5Y neuroblastoma cells, the unaggregated $A\beta_{1-42}$ film was dissolved in DMSO, then the solution was diluted in PBS. The purpose was to have the shift towards the β-sheet structure, which eventually leads to oligomerization and insoluble fibril formation, only during the incubation with the differentiated neuroblastoma cells.

3.2 Lipidomics and lipid identification

After incubation of the SH-SY5Y cells with the peptide, the lipid extraction of washed cells was performed by using a monophasic solvent extraction protocol with IPA 90 %, as previously reported [26]. It represents a convenient, less time consuming, less toxic and cheaper protocol in comparison to extraction methods performed with methyl tert-butyl ether (MTBE), Chloroform/MeOH ($CHCl_3$) such as of the classical Folch and Bligh & Dyer protocols. This method produced an improved yield of recovery and higher precision, accuracy and reproducibility, especially for more polar lipids.

For the analysis of the lipid extract, RP-type UHPLC lipid species separation was selected and coupled to ESI-QTOF-MS/MS detection. Data-independent SWATH acquisition provided comprehensive MS1 and MS2 data across all studied samples.

This lipidomic approach appeared sensible, reproducible, accurate and fast. The sample preparation required about 1.5 hour for the extraction and then the extracts, left drying during the night, could be analysed by the LC-MS in only 15 min per sample.

Afterwards, data were subjected to untargeted data processing. MS-DIAL software (setting parameters as previously specified) was utilized for peak finding, deisotoping, adduct annotation, alignment, MS2 spectra deconvolution, automated identification (via spectral matching of deconvoluted MS2 spectra against the *in silico* spectra of the LipidBlast database) and assessment of annotations via scoring functions. Data processed were then exported as peak list with peak heights and were then normalized by use of internal standards. The structural assignments of the most abundant lipids were afterwards confirmed through the evaluation of peak spotting plots of m/z vs RT.

It is known that lipid species of the distinct lipid classes elute in regular patterns in accordance with the homology principle; lipids with more double bonds elute earlier while lipids with longer acyl chains elute later always shifted by regular increments per structural repeat element if the gradient is linear. Hence, this empirical correlation was helpful to identify structural mis-annotations. It was based on the most abundant, easily identified lipids in each class, or on the added internal standards.

The lipid composition of SH-SY5Y cells, is still not yet known in detail. In 2019, for the first time, Halskau research group characterized the whole cell and plasma membrane lipid isolated from the neuroblastoma cell line SH-SY5Y [27]. In the same year, Xicoy et al. performed a lipidomic study, based on LC-MS analysis to determine Parkinson Disease-linked changes in the lipid profile of SH-SY5Y cell line, in that case treated with the neurotoxin 6-hydroxydopamine (6-OHDA) to confirm the validity of cultured 6-OHDA-treated SH-SY5Y cells as an attractive cell model for in *vitro* studies on PD [21]. In our study, 138 lipids from 9 lipid classes were identified in SH-SY5Y cell culture, normally used to study neurodegeneration and for evaluation of active compounds capable of halting amyloid toxicity.

Regarding the distribution of all identified lipid species according to their lipid classes, most of the lipids belonged to Phosphatidylcholines (PCs), that covered 35.5 % of all identified lipids (both polarities combined) (Fig.S1 S.I.). SMs were detected in the positive mode in a lower percentage distribution (10.9 %) in comparison to what has been reported in the work of Jacubeck [27]. Moreover, we were unable to identify the exact SMs FA acid composition because most observed

SM lipid species lacked FA-specific fragments. The latter finding is in line with a previous ^{31}P NMR phospholipid analysis of SH-SY5Y whole cell and plasma membrane lipid isolated. The abundance of PEs is lower than the one reported by Jakubec et al. (5.8%). Other widely identified lipid classes were Lyso-Phosphatidylcholines (LPCs) (15.9%) Triglycerides (TGs) (14.5%) and Ether-Phosphatidylcholines (PC-O) (11.6%), not described in their study. Moreover, a small number of Ceramides (Cers) (2.2%), Diglycerides (DGs) (1.4%) and Phosphatidylinositols (PIs) (2.2%) were detected as well. For future studies, the number of cells used for lipid extraction should be further increased to extend the lipid coverage of the current SH-SY5Y neuronal cell model.

3.2 Relative quantification of lipids

Thus, starting from evidence collected in previous lipidomic analysis in AD patients [28], in this preliminary work, we focused the relative quantification on the lipid classes of Phosphatidylcholine (PC), Lyso-Phosphatidylcholine (LPC) and Sphingomyelins (SM), because glycerophospholipids (GPs) and sphingolipids (SPs) perturbation, more than others, seems to be associated with neuronal injury, neuroinflammation and neurodegeneration [28]. In fact, it seems that PC depletion could identify cognitively normal individuals who will convert to AD within 2-3 years [29].

According to these prior evidences, in the present study, a significant decrease in percentage distribution of the following PCs species: PC (18:1-16:2); PC (18:0-20:3); PC (18:0-20:4); PC (16:0-22:5) and PC (16:0-22:6) was measured when differentiated neuroblastoma cells were treated with low (2-10 µM) and medium concentration (10-25 µM) of $A\beta_{1-42}$ peptide for 24 h [Fig. 3. (A)].

The results from the first case study [$A\beta_{1-42}$ (2-50 uM) treatment for 24 h] are in agreement with these previous findings [28]. In fact, the PC species that decreased their percentage distribution were those containing PUFA while the PC species that increased were those containing saturated FAs or MUFAs [Fig.3. (A)]. A concomitant correlated increased percentage for the MUFA-containing LPC species can be found: LPC 16:0 (1) (sn1 lyso form), LPC 16:0 (2) (sn2 lyso form), LPC 18:0 and a diminished percentage for PUFA-containing LPC [Fig.4. (A)]. These results are in line with accumulation of free PUFAs and Lyso-Phosphatidylcholine containing a saturated or monounsaturated FA in the sn-1 position reported in Palavicini's study [30].

In the second case study in which the same numbers of cells were incubated with $A\beta_{1-42}$ peptide at 50 µM for a longer time (48 h), the $A\beta_{1-42}$ determined a substantial toxic effect and cell death [Fig.

1. (B)]. A decrease of the percentage distribution of the following PCs species: PC (18:0-18:1); PC (18:1-18:1); PC (18:0-20:4) and PC (16:0-22:5) [Fig. 3. (B)] and an increase of saturated FAs containing LPC species: LPC 16:0; LPC 18:0 [Fig. 4 (B)] was observed.

These results are relevant considering the awareness that the dysregulated lipid homeostasis contributes greatly to the pathogenesis of AD. In fact, FAs and their metabolites are involved in synaptic plasticity, inflammation, cerebrovascular function and oxidative stress. In particular, a recent study demonstrated that oligomeric Aβ peptide induces accumulation of free PUFAs and Lyso-Phosphatidylcholine containing a saturated or monounsaturated FA in the sn-1 position [30]. This seems due to the activation of cytosolic phospholipase A2 (cPLA2), that in the presence of Ca^{2+} gets activated and binds to substrates in the cell membrane. It is highly specific for PC cleavage and arachidonic acid (AA) release (Fig.5) [30].

In addition, the metabolism of sphingolipids seems involved in AD pathogenesis as well, especially ceramides that consist of a sphingosine backbone and a fatty acid residue determine neuroinflammation and pro-apototic signal [31,32].

Concerning SMs, they are the most abundant SPs in the brain and they are important components of lipid rafts. We found decreased level of SMs and increased amount of ceramides content in SH-SY5Y samples treated with Aβ1-42 peptide. In particular, the SM 38:1;2O; SM 40:1;2O; SM 41:1;2O have a reduced percentage distribution under low and medium $A\beta_{1-42}$ peptide treatment for 24 h; SM 42:1;2O species is decreased as well at high $A\beta_{1-42}$ peptide treatment concentration for 24 h [Fig.6 (A)] while the percentage distribution of Cer 36:1;2O [Fig.7(A)] seems significantly elevated increasing the Aβ1-42 peptide concentration treatment.

In the second case study a decreased distribution of SM 40:1;2O, SM 42:1; 2O [Fig.6 (B)] was determined and a correlated elevated distribution of Cer 36:1;2O [Fig.7 (B)].

Our findings seem in line to studies on mouse model [33]: intracerebral injection of Aβ promoted neutral Sphingomyelinase (SMase) activity and increased ceramide levels. SMase is the enzyme responsible of catalysing the hydrolysis of phosphodiester bond in SM that results in the formation of phosphocholine and ceramide (Cer) (Fig.8). On the base of the optimal pH working condition, SMases are classified into three subtypes: acid, neutral, and alkaline; among these the acid SMase (ASM) and neutral SMase (NSM) are the main forms involved in Cer production in case of stress condition. Cer is a lipid mediator that can regulate cell growth and apoptosis. In particular, increased

levels of Cers due to NSM induction bring about a higher exosome secretion, that is known to be related to Aβ production, clearance and accumulation. In addition, exosomes are recognized as inflammatory mediators and crucial agents in oxidative stress during AD progression. Nowadays, it is confirmed that Aβ activates NSM but not ASM. However, ASM is associated with the onset of AD, especially when ASM activity is elevated the autophagy-lysosome pathway (ALP) is altered, autophagy degradation is reduced and so the misfolded proteins tend to accumulate. For this reasons, in clinical treatments the interest towards NSM and ASM as targets is increasing also in the field of AD [34].

4. Conclusions

This proposed method was found suitable to monitor some lipid metabolism alterations that might be correlated to $A\beta_{1-42}$ oligomers toxicity. The obtained results showed potential biomarkers for targeting and testing AD by *in vitro* cell assays.

The major alterations were found in PC and LPC level. We suppose that these might be due to the activation of Phospholipase A2 (PLA2) enzymes that hydrolyse the sn-2 ester bond of the membrane glycerophospholipids to generate MUFAs containing Lyso-phospholipids and polyunsaturated fatty acids (PUFAs). Both are biologically active lipid mediators, in particular arachidonic acid that plays a critical central role in neuroinflammation.

Concerning the alterations in the SM profile, we hypothesised the activation of the neutral SM-degrading enzyme Sphingomyelinase (SMase) that hydrolyses the phosphocholine-headgroup of Sphingomyelins producing proapoptotic ceramides. Moreover, recent studies have demonstrated the correlation between these enzymes and AD pathogenesis. Therefore, they could represent interesting targets for AD drug discovery.

This pilot work will guide future study designs for advanced investigations to validate the role of Aβ peptides on the lipidome of neuronal cells and the lipid biomarkers that could result in a more unambiguous AD diagnosis in plasma. Indeed, studies has confirmed that it is possible to examine brain-related alterations to lipid profiles in blood. In this view, further studies might involve the addition of amyloid aggregation and ß-secretase inhibitors in the SH-SY5Y cells culture incubated with amyloid. This investigation could be important to revert the amyloid toxic effects and verify the subsequent equilibration of these lipid alterations.

References:

[1] C.A. Lane, J. Hardy, J.M. Schott, Alzheimer's disease, Eur. J. Neurol. 25 (2018) 59-70

[2] C. Reitz, Alzheimer's disease and the amyloid cascade hypothesis: A critical review, Int. J. Alzheimers. Dis. 2012 (2012) 369808

[3] K. Hensley, J.M. Carney, M.P. Mattson, M. Aksenova, M. Harris, J.F. Wu, R.A. Floyd, D.A. Butterfield, A model for beta-amyloid aggregation and neurotoxicity based on free radical generation by the peptide: relevance to Alzheimer disease., Proc. Natl. Acad. Sci. U. S. A. 91 (1994) 3270–4

[4] A. Relini, N. Marano, A. Gliozzi, Probing the interplay between amyloidogenic proteins and membranes using lipid monolayers and bilayers, Adv. Colloid Interface Sci. 207 (2014) 81-92

[5] C. Fabiani, S.S. Antollini, Alzheimer's disease as a membrane disorder: Spatial cross-talk among beta-amyloid peptides, nicotinic acetylcholine receptors and lipid rafts, Front. Cell. Neurosci. 13 (2019) 309

[6] T.B. Zhu, Z. Zhang, P. Luo, S.S. Wang, Y. Peng, S.F. Chu, N.H. Chen, Lipid metabolism in Alzheimer's disease, Brain Res. Bull. 144 (2019) 68-74

[7] M. Cuperlovic-Culf, A. Badhwar, Recent advances from metabolomics and lipidomics application in alzheimer's disease inspiring drug discovery, Expert Opin. Drug Discov. 15 (2020) 319-331

[8] C. Gonzalez-Riano, A. Garcia, C. Barbas, Metabolomics studies in brain tissue: A review, J. Pharm. Biomed. Anal. 130 (2016) 141-168

[9] S. Akyol, Z. Ugur, A. Yilmaz, I. Ustun, S.K.K. Gorti, K. Oh, B. McGuinness, P. Passmore, P.G. Kehoe, M.E. Maddens, B.D. Green, S.F. Graham, Lipid profiling of Alzheimer's disease brain highlights enrichment in glycerol(Phospho)lipid, and sphingolipid metabolism, Cells. 10 (2021) 2591

[10] L.G. Zarrouk A, Debbabi M, Bezine M, Karym EM, Badreddine A, Rouaud O, Moreau T, Cherkaoui-Malki M, El Ayeb M, Nasser B, Hammami M, Lipid Biomarkers in Alzheimer's Disease, 15 (2018) 303–312.

[11] M.W. Wong, N. Braidy, A. Poljak, R. Pickford, M. Thambisetty, P.S. Sachdev, Dysregulation of lipids in Alzheimer's disease and their role as potential biomarkers, Alzheimer's Dement. 13 (2017) 810-827

[12] A. Naudí, R. Cabré, M. Jové, V. Ayala, H. Gonzalo, M. Portero-Otín, I. Ferrer, R. Pamplona, Lipidomics of Human Brain Aging and Alzheimer's Disease Pathology, in: Int. Rev. Neurobiol. 122 (2015) 133-189

[13] M. Agarwal, S. Khan, Plasma Lipids as Biomarkers for Alzheimer's Disease: A Systematic Review, Cureus. 12 (2020) e12008.

[14] B. Burla, M. Arita, M. Arita, A.K. Bendt, A. Cazenave-Gassiot, E.A. Dennis, K. Ekroos, X. Han, K. Ikeda, G. Liebisch, M.K. Lin, T.P. Loh, P.J. Meikle, M. Orešič, O. Quehenberger, A. Shevchenko, F. Torta, M.J.O. Wakelam, C.E. Wheelock, M.R. Wenk, MS-based lipidomics of human blood plasma: A community-initiated position paper to develop accepted guidelines, J. Lipid Res. 59 (2018) 2001-2017

[15] M. Bartolini, M. Naldi, J. Fiori, F. Valle, F. Biscarini, D. V. Nicolau, V. Andrisano, Kinetic characterization of amyloid-beta 1-42 aggregation with a multimethodological approach, Anal. Biochem. 414 (2011) 215-225.

[16] A. De Simone, M. Naldi, D. Tedesco, A. Milelli, M. Bartolini, L. Davani, D. Widera, M.L. Dallas, V. Andrisano, Investigating in vitro amyloid peptide 1−42 aggregation: Impact of higher molecular weight stable adducts, ACS Omega. 4 (2019) 12308–12318

[17] B. Drotleff, J. Illison, J. Schlotterbeck, R. Lukowski, M. Lämmerhofer, Comprehensive lipidomics of mouse plasma using class-specific surrogate calibrants and SWATH acquisition for large-scale lipid quantification in untargeted analysis, Anal. Chim. Acta. 1086 (2019) 90-102

[18] H. Tsugawa, T. Cajka, T. Kind, Y. Ma, B. Higgins, K. Ikeda, M. Kanazawa, J. Vandergheynst, O. Fiehn, M. Arita, MS-DIAL: Data-independent MS/MS deconvolution for comprehensive metabolome analysis, Nat. Methods. 12 (2015) 523–526

[19] F. dos S. Petry, B.P. Coelho, M.M. Gaelzer, F. Kreutz, F.T.C.R. Guma, C.G. Salbego, V.M.T. Trindade, Genistein protects against amyloid-beta-induced toxicity in SH-SY5Y cells by regulation of Akt and Tau phosphorylation, Phyther. Res. 34 (2019) 796-807

https://doi.org/10.1002/ptr.6560.

[20] H. Wang, J. Ma, Y. Tan, Z. Wang, C. Sheng, S. Chen, J. Ding, Amyloid-β1-42M induces reactive oxygen species-mediated autophagic cell death in U87 and SH-SY5Y cells, J. Alzheimer's Dis. 21 (2010) 597–610. ì

[21] H. Xicoy, J.F. Brouwers, O. Kalnytska, B. Wieringa, G.J.M. Martens, Lipid Analysis of the 6-Hydroxydopamine-Treated SH-SY5Y Cell Model for Parkinson's Disease, Mol. Neurobiol. 57 (2020) 848–859..

[22] M.M. Shipley, C.A. Mangold, M.L. Szpara, Differentiation of the SH-SY5Y human neuroblastoma cell line, J. Vis. Exp. 17 (2016) 53193

[23] J. Krishtal, O. Bragina, K. Metsla, P. Palumaa, V. Tõugu, In situ fibrillizing amyloid-beta 1-42 induces neurite degeneration and apoptosis of differentiated SH-SY5Y cells, PLoS One. 12 (2017) e0186636

[24] M.P. Lambert, G. Stevens, S. Sabo, K. Barber, G. Wang, W. Wade, G. Krafft, S. Snyder, T.F. Holzman, W.L. Klein, β/A4-evoked degeneration of differentiated SH-SY5Y human neuroblastoma cells, J. Neurosci. Res. 39 (1994) 377-385

[25] M. Bartolini, C. Bertucci, M.L. Bolognesi, A. Cavalli, C. Melchiorre, V. Andrisano, Insight into the kinetic of amyloid β (1-42) peptide self-aggregation: Elucidation of inhibitors' mechanism of action, ChemBioChem. 8 (2007) 2152-2161

[26] C. Calderón, C. Sanwald, J. Schlotterbeck, B. Drotleff, M. Lämmerhofer, Comparison of simple monophasic versus classical biphasic extraction protocols for comprehensive UHPLC-MS/MS lipidomic analysis of Hela cells, Anal. Chim. Acta. 1048 (2019) 66-74.

[27] M. Jakubec, E. Bariås, F. Kryuchkov, L.V. Hjørnevik, Ø. Halskau, Fast and Quantitative Phospholipidomic Analysis of SH-SY5Y Neuroblastoma Cell Cultures Using Liquid Chromatography-Tandem Mass Spectrometry and 31P Nuclear Magnetic Resonance, ACS Omega. 4 (2019) 21596–21603.

[28] Y.C. Kao, P.C. Ho, Y.K. Tu, I.M. Jou, K.J. Tsai, Lipids and alzheimer's disease, Int. J. Mol. Sci. 21 (2020) 1505

[29] M. Mapstone, A.K. Cheema, M.S. Fiandaca, X. Zhong, T.R. Mhyre, L.H. Macarthur, W.J. Hall,

S.G. Fisher, D.R. Peterson, J.M. Haley, M.D. Nazar, S.A. Rich, D.J. Berlau, C.B. Peltz, M.T. Tan, C.H. Kawas, H.J. Federoff, Plasma phospholipids identify antecedent memory impairment in older adults, Nat. Med. 20 (2014) 415–418

[30] J.P. Palavicini, C. Wang, L. Chen, K. Hosang, J. Wang, T. Tomiyama, H. Mori, X. Han, Oligomeric amyloid-beta induces MAPK-mediated activation of brain cytosolic and calcium-independent phospholipase A2 in a spatial-specific manner, Acta Neuropathol. Commun. 5 (2017) 56

[31] M. Kosicek, S. Hecimovic, Phospholipids and Alzheimer's disease: Alterations, mechanisms and potential biomarkers, Int. J. Mol. Sci. 14 (2013) 1310-1322

[32] L.M. Munter, The lipid component of Alzheimer's disease research, J. Neurochem. 154 (2020) 7-10.

[33] A. V. Alessenko, A.E. Bugrova, L.B. Dudnik, Connection of lipid peroxide oxidation with the sphingomyelin pathway in the development of Alzheimer's disease, in: Biochem. Soc. Trans 32 (2004) 144-6.

[34] H. Xiang, S. Jin, F. Tan, Y. Xu, Y. Lu, T. Wu, Physiological functions and therapeutic applications of neutral sphingomyelinase and acid sphingomyelinase, Biomed. Pharmacother. 139 (2021) 111610.

.

Figure captions:

Fig. 1. Percentage Viability of SH-SY5Y cells treated with $A\beta_{1-42}$. SH-SY5Y cells were incubated with Aβ1-42 (A) at increasing concentrations (2-50 µM) for 24 h (B) at highest concentration (50 µM) for 48 h. Data are expressed as percentage with respect to untreated cells, considered as 100 % cell viability. Each bar represents means ± SEM of three independent experiments

Fig. 2. Lipid identification: Peak spotting map. (A) corresponds to the spotting map of the lipid species identified in positive ionization mode (ESI+), while (B) depicts the lipid species determined in negative ionization mode.

Fig. 3 Relative Phosphatidylcholine (PC) distribution in the lipid extract of differentiated. SH-SY5Y cells treated with Aβ1-42 SH-SY5Y cells were incubated with $A\beta_{1-42}$ (A) at increasing concentration (2-50 μM) for 24 h (B) at highest concentration (50 μM) for 48 h. Each bar represents means ± SEM of three independent experiments.

Fig. 4. Relative Lyso-phosphatidylcholine (LPC) distribution distribution in the lipid extract of differentiated SH-SY5Y cells treated with $A\beta_{1-42}$. SH-SY5Y cells were incubated with $A\beta_{1-42}$ (A) at increasing concentration (2-50 μM) for 24 h (B) at highest concentration (50 μM) for 48 h. Each bar represents means ± SEM of three independent experiments

Fig. 5. Cytosolic phospholipase A2 (cPLA2) catalyses PC cleveage at sn-2 position. PUFAs and Lyso-Phosphatidylcholine containing a saturated or monounsaturated FA in the sn-1 position are released

Fig. 6. Relative Sphingomyelin (SM) distribution in the lipid extract of differentiated SH-SY5Y cells treated with $A\beta_{1-42}$. SH-SY5Y cells were incubated with $A\beta_{1-42}$ (A) at increasing concentration (2-50 μM) for 24 h (B) at highest concentration (50 μM) for 48 h. Each bar represents means ± SEM of three independent experiments.

Fig. 7. Relative Ceramide (Cer) distribution in the lipid extract of differentiated SH-SY5Y cells treated with $A\beta_{1-42}$. SH-SY5Y cells were incubated with $A\beta_{1-42}$ (A) at increasing concentration (2-50 μM) for 24 h (B) at highest concentration (50 μM) for 48 h. Each bar represents means ± SEM of three independent experiments.

Fig. 8. Sphingomyelinase (SMase) catalyses sphingomyelin to ceramide by hydrolysis.

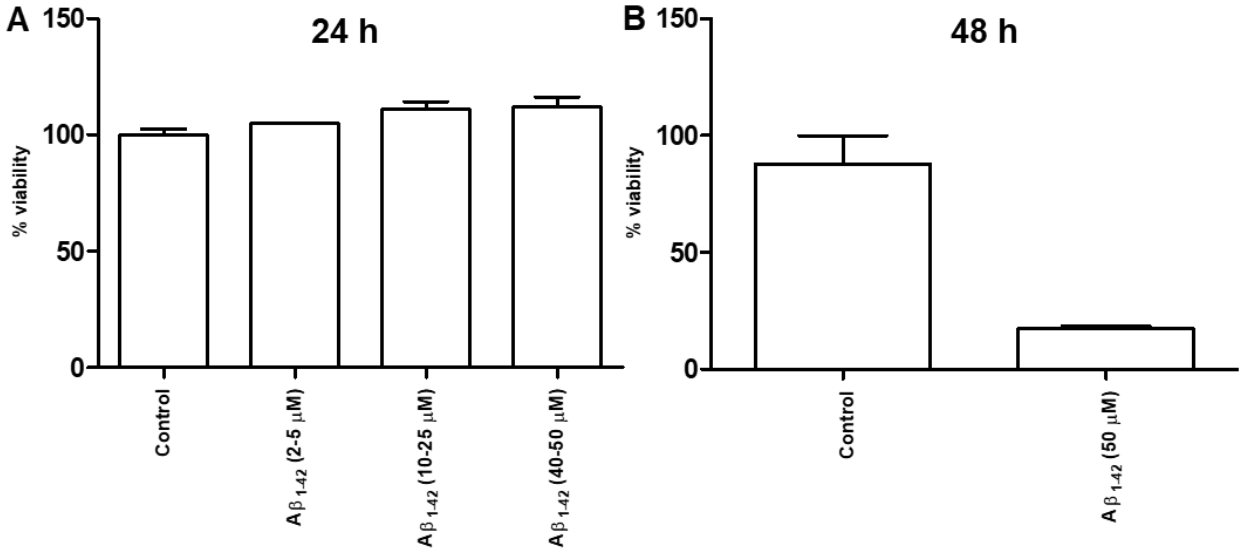
A
24 h
150
100
50
0
% viability
Control
Aβ 1-42 (2-5 μM)
Aβ 1-42 (10-25 μM)
Aβ 1-42 (40-50 μM)
B
48 h
150
100
50
0
% viability
Control
Aβ 1-42 (50 μM)

Fig.1

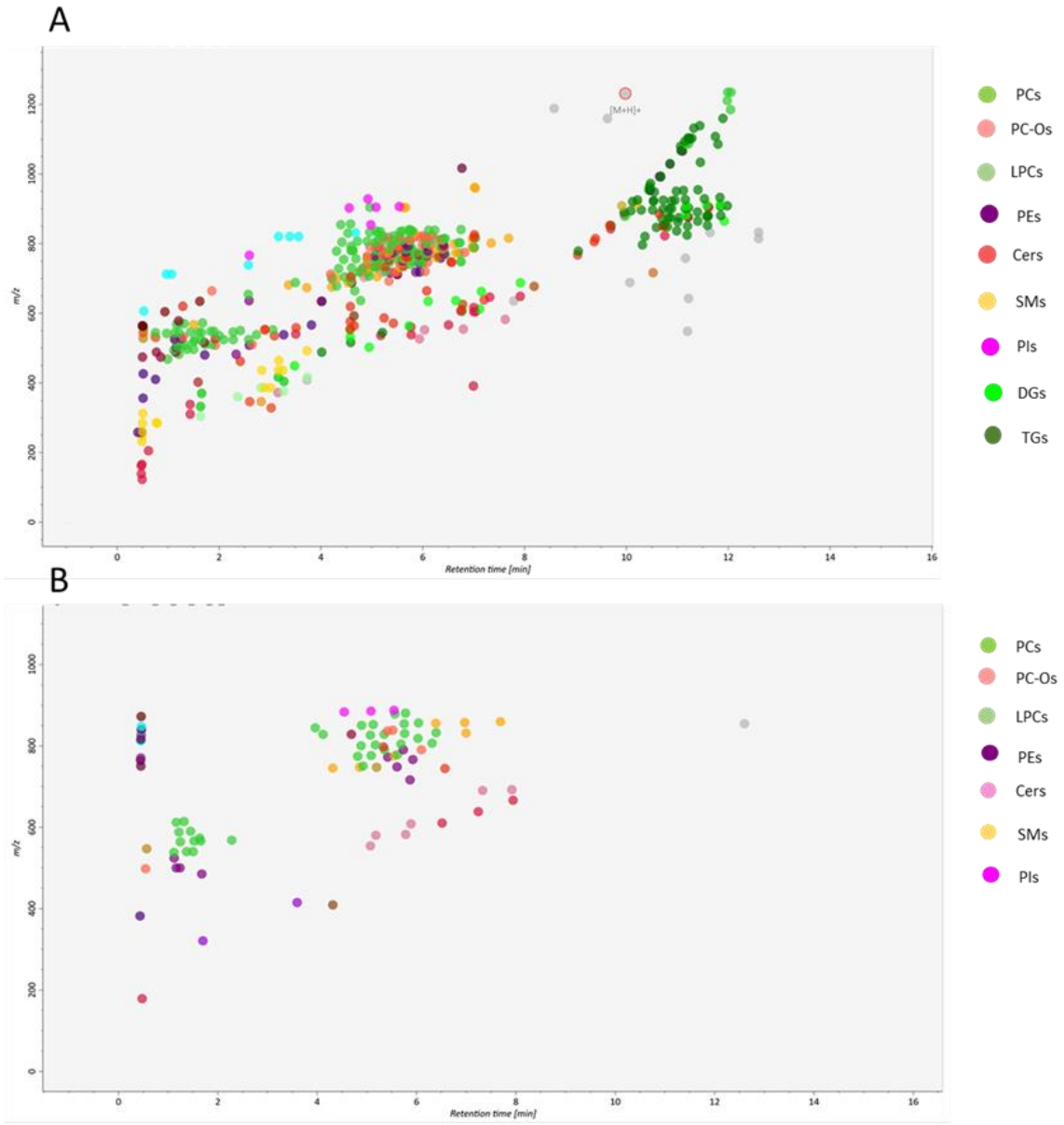
A
[M+H]+
m/z
Retention time [min]
PCs
PC-Os
LPCs
PEs
Cers
SMs
PIs
DGs
TGs
B
m/z
Retention time [min]
PCs
PC-Os
LPCs
PEs
Cers
SMs
PIs

Fig.2

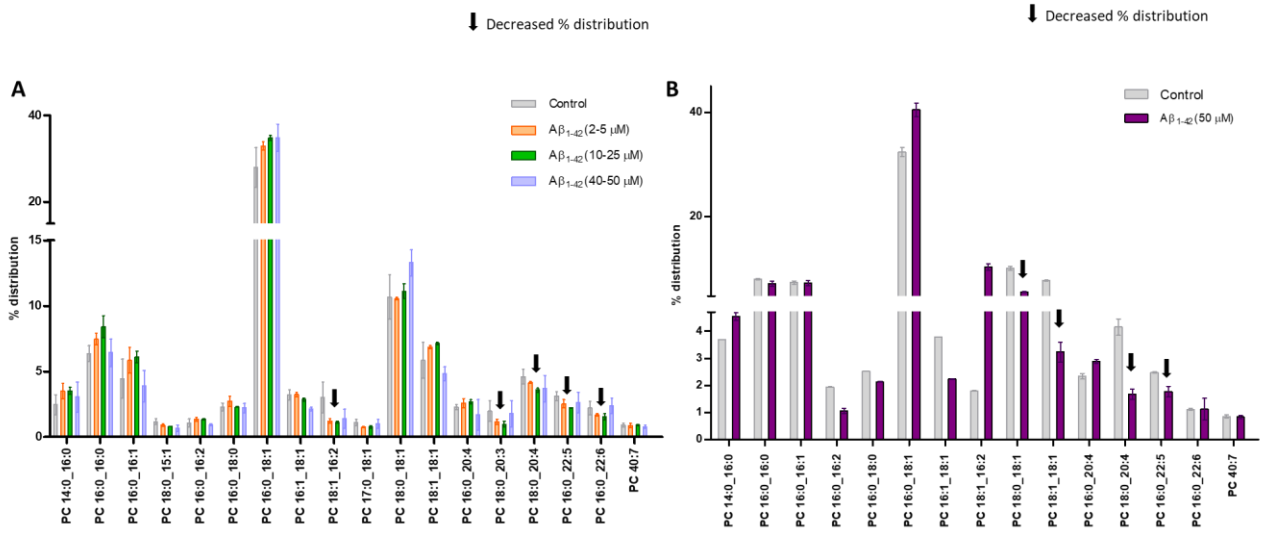
Decreased % distribution
A
Control
Aβ1-42 (2-5 μM)
Aβ1-42 (10-25 μM)
Aβ1-42 (40-50 μM)
% distribution
PC 14:0_16:0
PC 16:0_16:0
PC 16:0_16:1
PC 18:0_15:1
PC 16:0_16:2
PC 16:0_18:0
PC 16:0_18:1
PC 16:1_18:1
PC 18:1_16:2
PC 17:0_18:1
PC 18:0_18:1
PC 18:1_18:1
PC 16:0_20:4
PC 18:0_20:3
PC 18:0_20:4
PC 16:0_22:5
PC 16:0_22:6
PC 40:7
Decreased % distribution
B
Control
Aβ1-42 (50 μM)
% distribution
PC 14:0_16:0
PC 16:0_16:0
PC 16:0_16:1
PC 16:0_16:2
PC 16:0_18:0
PC 16:0_18:1
PC 16:1_18:1
PC 18:1_16:2
PC 18:0_18:1
PC 18:1_18:1
PC 16:0_20:4
PC 18:0_20:4
PC 16:0_22:5
PC 16:0_22:6
PC 40:7

Fig.3

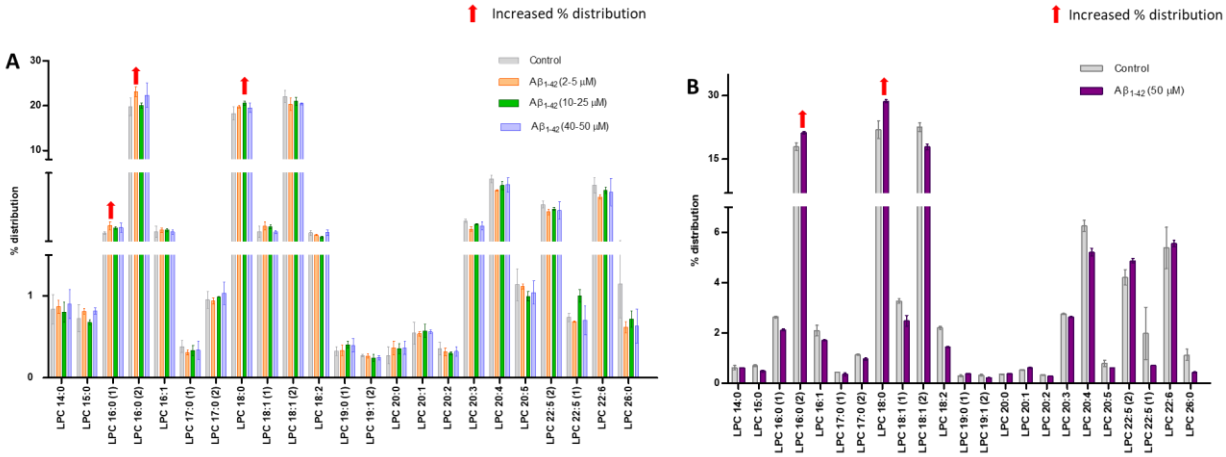
A
Increased % distribution
Control
Aβ1-42 (2-5 μM)
Aβ1-42 (10-25 μM)
Aβ1-42 (40-50 μM)
% distribution
LPC 14:0
LPC 15:0
LPC 16:0 (1)
LPC 16:0 (2)
LPC 16:1
LPC 17:0 (1)
LPC 17:0 (2)
LPC 18:0
LPC 18:1 (1)
LPC 18:1 (2)
LPC 18:2
LPC 19:0 (1)
LPC 19:1 (2)
LPC 20:0
LPC 20:1
LPC 20:2
LPC 20:3
LPC 20:4
LPC 20:5
LPC 22:5 (2)
LPC 22:5 (1)
LPC 22:6
LPC 26:0
B
Increased % distribution
Control
Aβ1-42 (50 μM)
% distribution

Fig.4

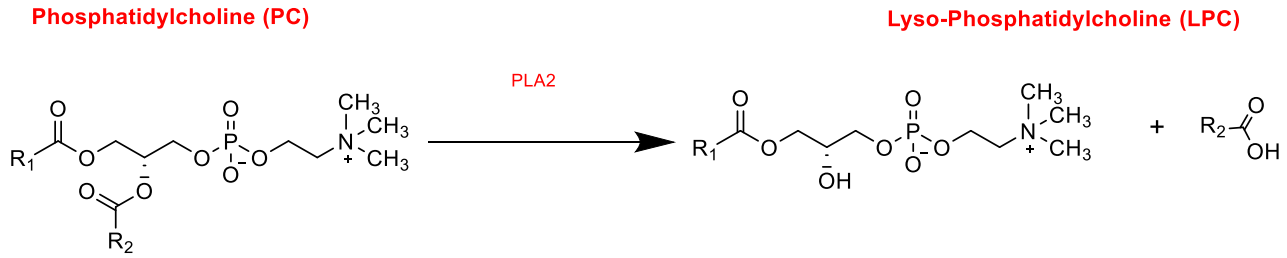
Phosphatidylcholine (PC)
Lyso-Phosphatidylcholine (LPC)
PLA2

Fig.5

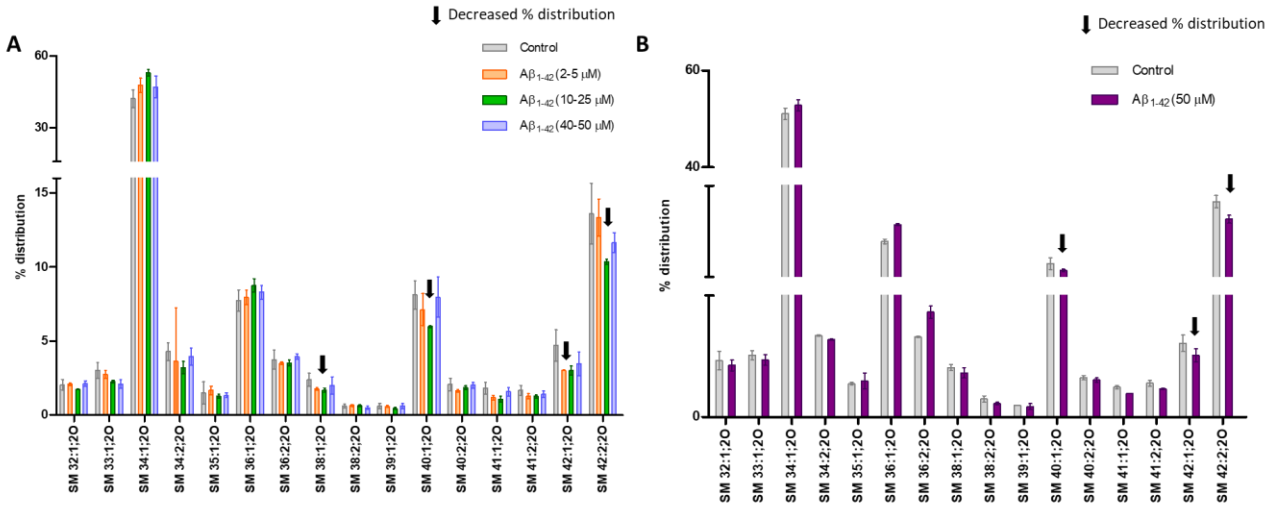
A
Decreased % distribution
Control
Aβ1-42(2-5 μM)
Aβ1-42(10-25 μM)
Aβ1-42(40-50 μM)
% distribution
SM 32:1;2O
SM 33:1;2O
SM 34:1;2O
SM 34:2;2O
SM 35:1;2O
SM 36:1;2O
SM 36:2;2O
SM 38:1;2O
SM 38:2;2O
SM 39:1;2O
SM 40:1;2O
SM 40:2;2O
SM 41:1;2O
SM 41:2;2O
SM 42:1;2O
SM 42:2;2O
B
Decreased % distribution
Control
Aβ1-42(50 μM)
% distribution
SM 32:1;2O
SM 33:1;2O
SM 34:1;2O
SM 34:2;2O
SM 35:1;2O
SM 36:1;2O
SM 36:2;2O
SM 38:1;2O
SM 38:2;2O
SM 39:1;2O
SM 40:1;2O
SM 40:2;2O
SM 41:1;2O
SM 41:2;2O
SM 42:1;2O
SM 42:2;2O

Fig.6

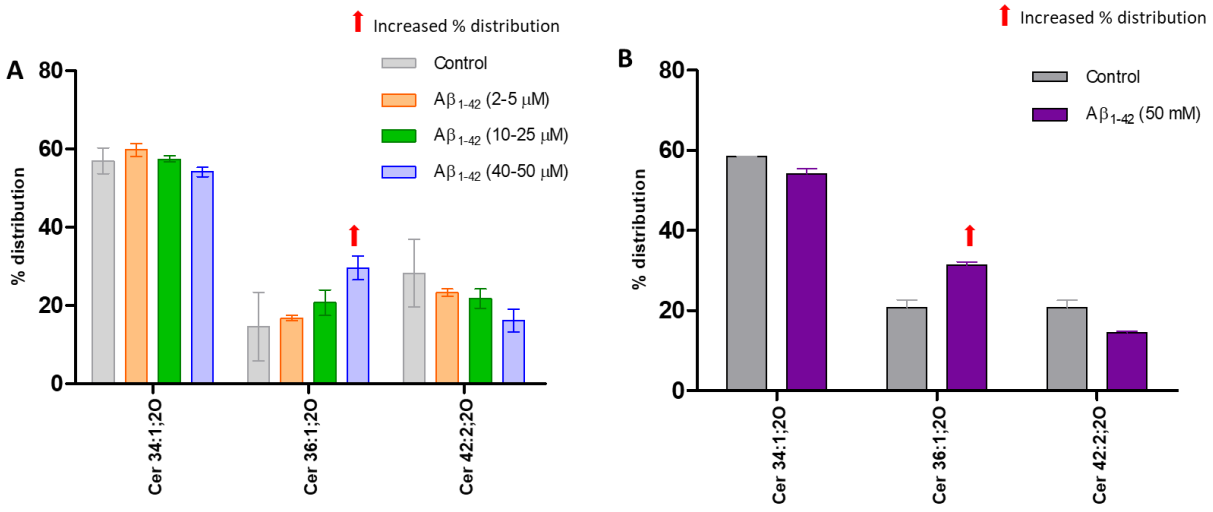
A
B
Increased % distribution
Control
Aβ1-42 (2-5 μM)
Aβ1-42 (10-25 μM)
Aβ1-42 (40-50 μM)
Aβ1-42 (50 mM)
% distribution
0
20
40
60
80
Cer 34:1;2O
Cer 36:1;2O
Cer 42:2;2O

Fig.7

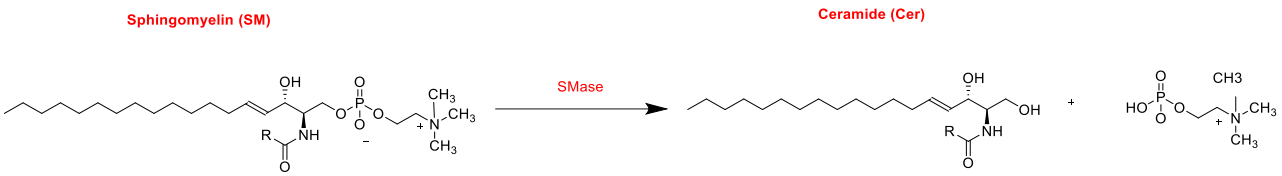

Fig.8